Supporting Information

Belcher et al. 10.1073/pnas.1011974107

SI Methods

Fire Invasion Model. We have constructed a cellular automaton model that simulates the propagation of a smoldering fire as a contact invasion process. The model is stochastic and intentionally simple so that it can be parameterized with the sparse data that are available on palaeoatmospheric fire activity. The model can be viewed as a simplification of other wildfire models that have been developed to simulated present-day forest fires (1 and 2).

We define the model on a 50×50 square grid, which will represent a physical area of 10×10 cm. Each grid square can be in one of three states: "available to burn," "burning," and "burned out." These three states are equivalent to the susceptible, infected, and recovered (SIR) states in an SIR epidemic model, and the model as a whole is analogous to a lattice gas cellular automaton of an SIR-type epidemic (3). Our model has two parameters: the probability of local fire spread β and the probability of local fire extinction μ. Each grid square has eight neighbors in a Moore neighborhood (Fig. S5). A grid square which is burning can ignite any neighboring square that is available to burn with the probability β per unit time step. In this way, the smoldering fire front spreads by a contact process. Other fire models have included long-range transmission of fire to nonneighboring locations. This long-range transmission, which represents processes such as burning embers and firebrands, is less applicable to smoldering fires and would require additional parameters that are not possible to collect from paleontological data.

We performed 10^6 simulations of this model with randomly selected values of β and μ from the ranges 0.005–0.05 and 0.01–0.2, respectively. From each simulation, we recorded the time taken for the fire to completely burn out (burn duration), the rate of spread of the fire across the arena (spread rate), and the final proportion of sites burned (burn probability). This set of parameters gives burn durations in the range of 10^{-4}–10^3 min and spread rates in the range 0–0.39 cm/min, which encompasses all the experimentally observed spread rates and burn durations and the predicted spread rates and burn durations for historical O_2 concentrations. Three example simulations are shown in Fig. 3 of the main article. The model output can be classed into two broad kinds of behavior: simulations where the fire spread across the entire model arena and simulations where the fire burned out before reaching spreading across the entire model arena. Fig. 3*A* is an example of the second type of behavior, and Fig. 3*B* and *C* show the first type of behavior.

The experimental data gives relationships for O_2 vs. spread rate and O_2 vs. burn duration,

$$\text{Burn duration (mins)} = 26(\pm 5)O_2 - 380(\pm 100)$$

and

$$\text{Spread Rate (cm/min)} = 0.011(\pm 0.006)O_2 - 0.15(\pm 0.11),$$

where the numbers following $\pm$ give the standard error. We selected all simulations that lay within 20% of the predicted spread rate and burn duration for a given level of O_2. The distribution of fire activity at this level of O_2 was then obtained from the proportions of sites burned for these selected simulations. For example, at 20% O_2 the linear regressions from the experimental data predict a burn duration of 145 min and a spread rate of 0.076 cm/min. We would therefore select all simulations with burn durations in the range 116–174 min and spread rates in the range 0.06–0.09. These selected simulations then give us a distribution of simulation parameters (Fig. S6 *A* and *B*) and a distribution of burn probabilities (Fig. 6*C*).

The distribution of parameter values (Fig. S7) and burn probabilities (Fig. 4 of main article) can then be calculated for a range of O_2 concentrations between 16 and 26%. The final relationship between O_2 and burn probability has a nonlinear relationship with the experimental results. If the experimental results had given different relationships between burn duration and spread rate, then completely different patterns between O_2 and burn probability are possible (Fig. S8).

1. Alexandridis A, Vakalis D, Siettos CI, Bafas GV (2008) A cellular automata model for forest fire spread prediction: The case of the wildfire that swept through Spetses Island in 1990. *Appl Math Comput* 204:191–201.
2. Encinas AH, Encinas LH, White SH, del Rey AM, Sanchez GR (2007) Simulation of forest fire fronts using cellular automata. *Adv Eng Softw* 38:372–378.
3. Karafyllidis I, Thanailakis A (1997) A model for predicting forest fire spread using cellular automata. *Ecol Model* 6:191–200.

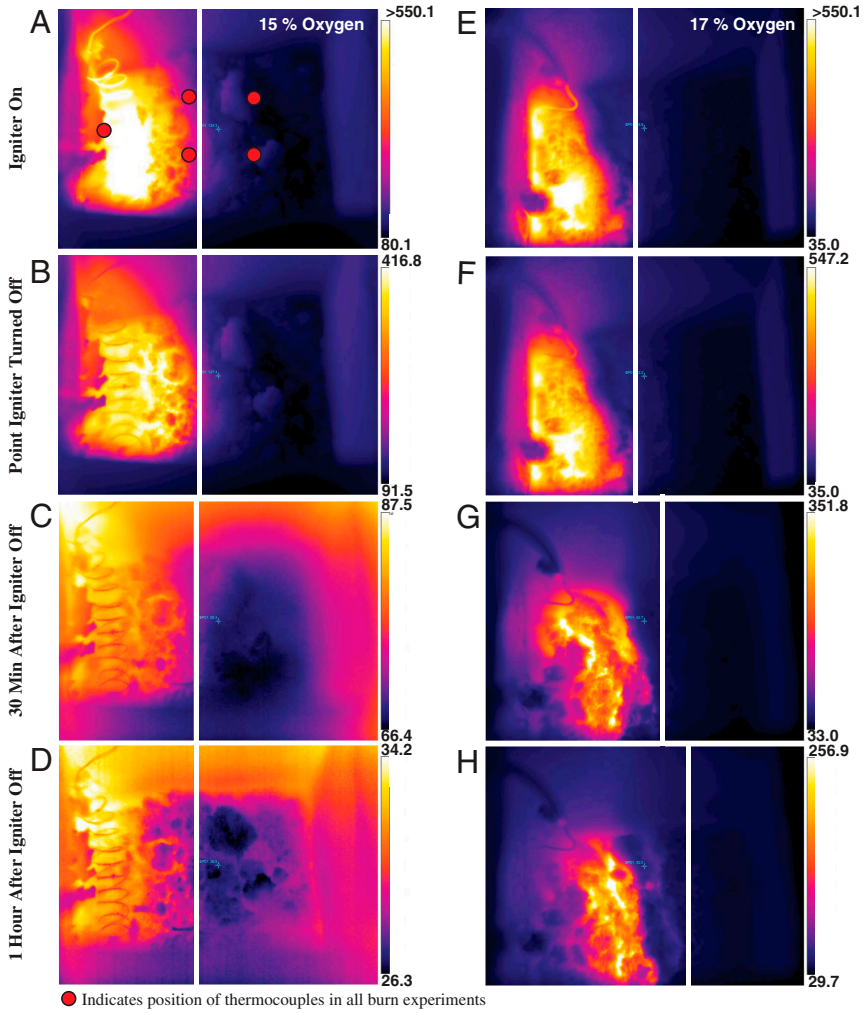

Fig. S1. Thermal images showing movement of the thermal front (highlighted by white bar drawn through the images). *A–D* results in 15% O_2, *E–H* results in 17% O_2. *A* and *E* show the thermal front during ignitor on. *B* and *F* show the point at which the igniter is turned off. *C* and *G* show propagation of the thermal front and temperatures 30 min after the igniter was turned off. *D* and *H* show propagation of the thermal front and temperatures 1 h after the igniter was turned off. High temperatures remain in the experimental run in 17% O_2, and propagation can be observed in the thermal front. Temperatures plummet rapidly on coil shutdown in 15% O_2 and no propagation is observed. Note the change in temperature scales on each image.

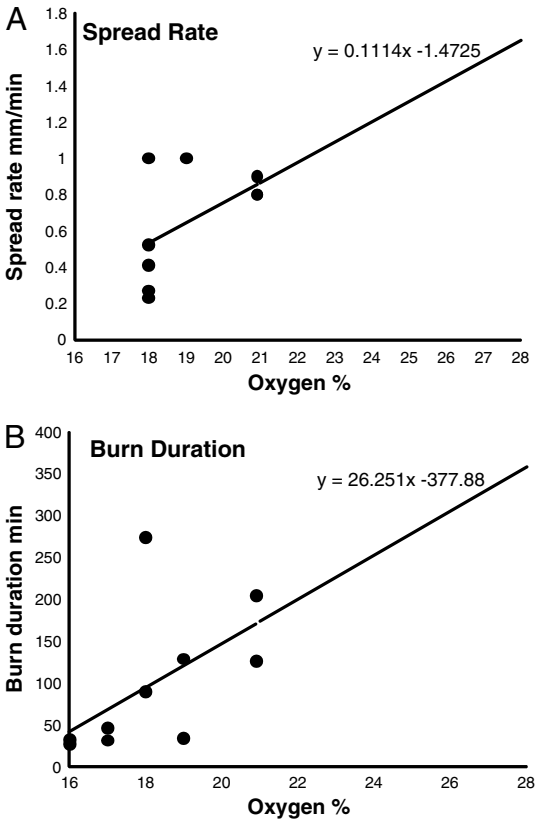

Fig. S2. Spread rates and burn duration derived from the self-supporting combustion experiments. (*A*) Spread rates plotted as a function of atmospheric oxygen, revealing the relationship $SR = 0.011(\pm 0.006)O_2 - 1.5(\pm 0.11)$. (*B*) Burn duration as a function of atmospheric oxygen, revealing the relationship $t_{burn} = 26(\pm 5)O_2 - 380(\pm 100)$ (numbers in brackets are the standard error).

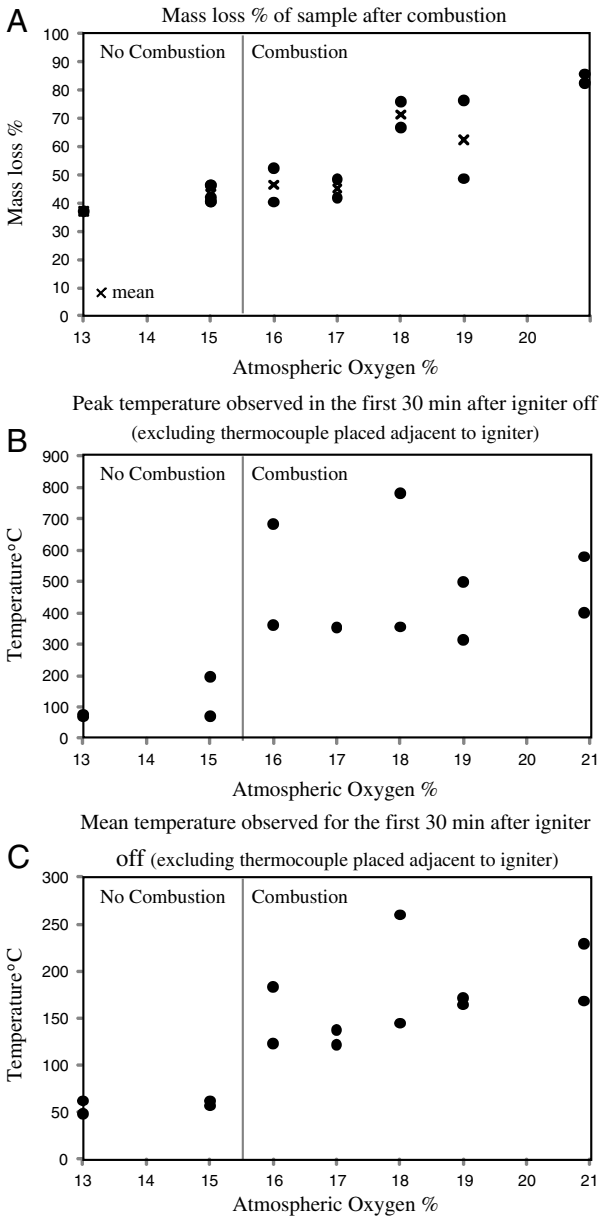

Fig. S3. Temperature and mass loss data from the self-supporting combustion experiments. (*A*) Mass lost (% of total) by the samples after combustion, showing only significant mass loss at 18% O_2 and above. (*B*) Peak temperature observed during the first 30 min after the igniter coil was turned off. (*C*) Mean temperature over the same period.

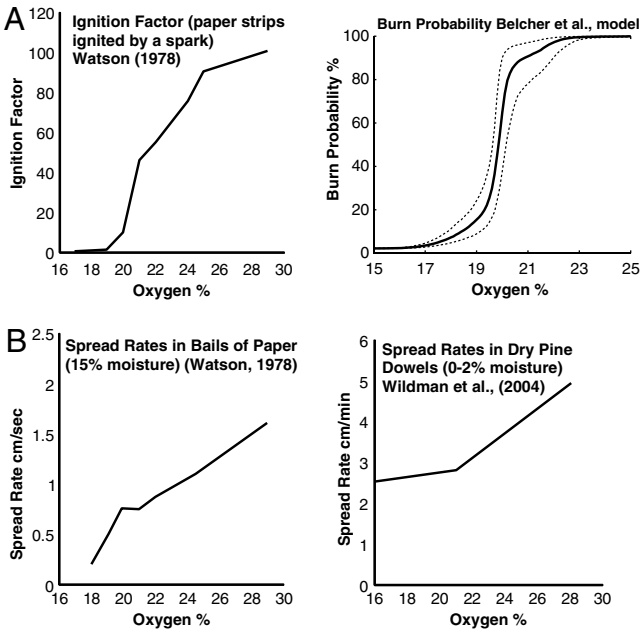

Fig. S4. Figures highlighting that our model is consistent with previous fire and oxygen observations. We reveal that fire activity/burn probability is dependent on O_2, which is consistent with *A*, which estimates ignition factor compared to oxygen (1). Watson's data revealed a rapid rise in ignition component with increasing atmospheric oxygen. The spread rates used in part to drive our model (see Fig S2) are also consistent with the observed near-linear increase in spread rate from refs. 1and 2, both shown in *B*. These highlight that both the underlying data used to drive our model and the output from it are well supported.

1 Watson AJ (1978) Consequences for the biosphere of forest and grassland fires. PhD thesis (University of Reading, Reading, UK).
2 Wildman RA, et al. (2004) Burning of forest materials under late Paleozoic high atmospheric oxygen levels. *Geology* 32:457–460.
3 Belcher CM, McElwain JC (2008) Limits for combustion in low O_2 redefine paleoatmospheric predictions for the Mesozoic. *Science* 321:1197–1200.

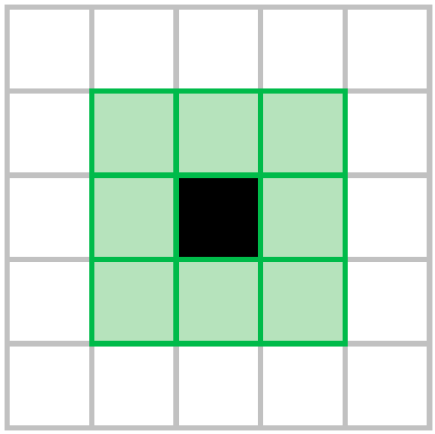

Fig. S5. The Moore neighborhood (green squares) of the central black square. Burning grid squares have a probability μ per unit time step of becoming burned out, which implies that the length of time that a grid square is in the burning state is geometrically distributed with a mean of $1/\mu$ time steps. We take one time step as being 6 s.

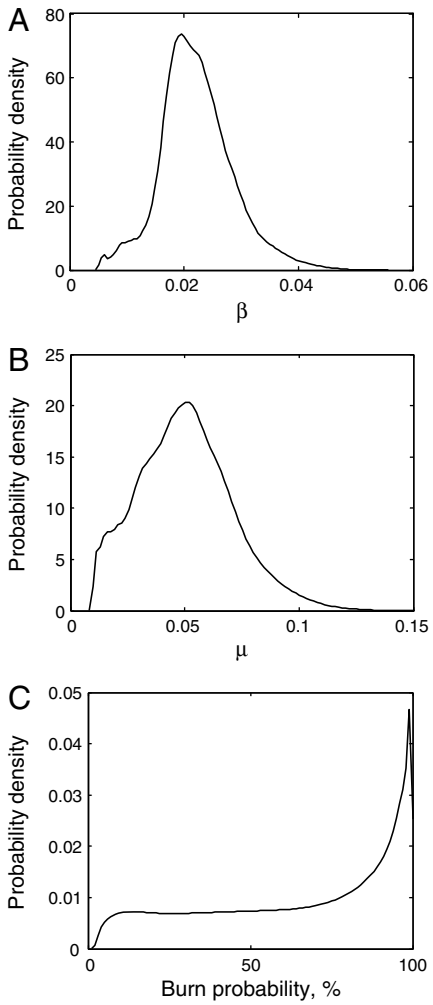

Fig. S6. The distributions of (*A*) model parameter β, (*B*) model parameter μ, and (*C*) burn probability distributions after selecting all simulations with burn durations in the range 116–174 min and spread rates in the range 0.06–0.09. These selected simulations are used to make model estimates for 20% O_2 concentration.

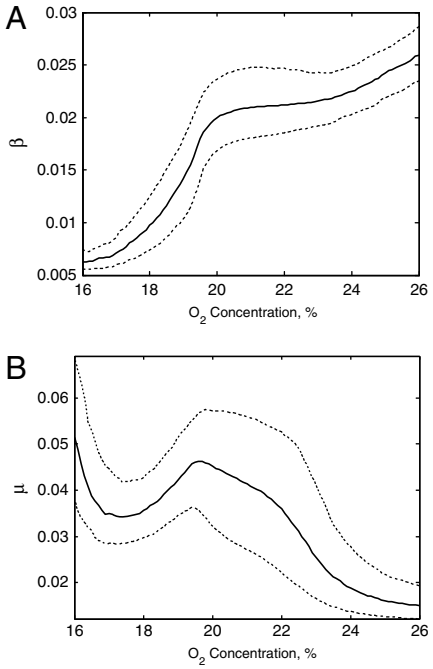

Fig. S7. The model-derived medians (solid line) and quantiles (dashed line) for β, μ, and burn probability across a range of O_2 concentrations.

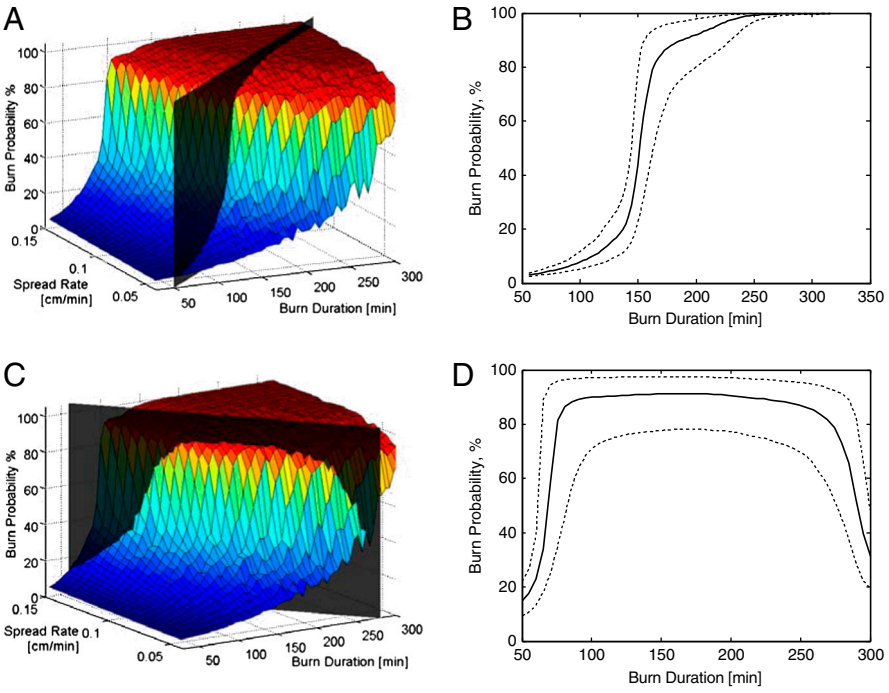

Fig. S8. (*A*) Median burn probabilities as modeled for a range parameter spread rates and burn durations. The experimentally derived relationship between spread rate and burn duration is shown as a dark plane cutting the parameter space. (*B*) Simulation results are selected that lie with 20% of this plane giving rise to a relationship between burn probability and burn duration. (*C*) A hypothetical relationship between burn duration and spread rate. (*D*) The resulting output relationship between burn duration and burn probability.